RSC Advances

PAPER

Check for updates

Cite this: RSC Adv., 2018, 8, 374

Synthesis of alloyed $Zn_{1-x}Mn_xS$ nanowires with completely controlled compositions and tunable bandgaps†

Jing Cai, *[a] Sheng Wang,[a] Kefu Zhu,[a] Yucheng Wu, *[a] Lizhao Zhou,[a] Yongliang Zhang,[a] Qiang Wu,[b] Xizhang Wang*[b] and Zheng Hu[b]

Received 23rd November 2017
Accepted 14th December 2017

DOI: 10.1039/c7ra12714f

rsc.li/rsc-advances

This study reported the successful synthesis of $Zn_{1-x}Mn_xS$ nanowires with completely controlled compositions ($0 \le x \le 1$); the x values could be well controlled by tuning the feeding ratio of $[(C_4H_9)_2NCS_2]_2Zn$ to $[(C_4H_9)_2NCS_2]_2Mn$ precursors. The bandgaps of $Zn_{1-x}Mn_xS$ nanowires showed nonlinear bowing character *versus* the composition. This result provided an effective route for designing Mn-based ternary chalcogenide nanowires with specific bandgaps, which is significant for their better application in photonics and spintronics.

Introduction

Mn^{2+} doped semiconductor nanomaterials have attracted great attention in photonics and spintronics due to their unique optical and magnetic properties,[1,2] such as orange photoluminescence emission[3,4] and photo-induced magnetization.[5] Many factors could affect their optical or magnetic properties, including the temperature,[4,6] dopant location[7,8] and composition/dopant concentration.[4,9–15] As is well known, the composition is a key factor affecting the bandgaps of semiconductor nanomaterials,[16–23] *e.g.* the ternary $Zn_xCd_{1-x}S$[16–18], CdS_xSe_{1-x}[19] and $ZnSe_xTe_{1-x}$[20] nanowires, all showed the tunable bandgaps *versus* the composition. Hence, the synthesis of composition completely controlled Mn-based ternary chalcogenide nanomaterials is significant to explore the relationship between their bandgaps and composition. Many methods have been employed to synthesize Mn^{2+} doped chalcogenide nanomaterials, such as the nucleation and growth doping methods[9] as well as the ionic diffusion and exchange doping methods,[13] however, it remains challenge for synthesizing composition completely controlled Mn-based ternary chalcogenide nanomaterials, especially for the one dimensional nanostructures such as $Zn_{1-x}Mn_xS$ nanowires.

The solution-solid-solid (SSS) growth has shown great convenience in synthesis of various binary chalcogenide nanowires[24–33] and even ternary $Zn_xCd_{1-x}S$[16,18] nanowires with superionic conductors such as Ag_2S, Ag_2Se and $Cu_{2-x}S$ as catalysts. Previously, we have synthesized the ZnS nanowires[16] and MnS nanowires[25] *via* the SSS route using Ag_2S nanoparticles as the catalysts, and the adopted precursors were metalorganic $[(C_4H_9)_2NCS_2]_2Zn$ and $[(C_4H_9)_2NCS_2]_2Mn$, respectively. The two precursors are of similar structures, and their decomposing rates and conditions might be similar, thus co-decomposing $[(C_4H_9)_2NCS_2]_2Zn$ and $[(C_4H_9)_2NCS_2]_2Mn$ was probably very suitable for the synthesis of composition completely controlled $Zn_{1-x}Mn_xS$ nanowires.

Herein, by adopting the $[(C_4H_9)_2NCS_2]_2Zn$ and $[(C_4H_9)_2NCS_2]_2Mn$ precursors with different molar ratios, we successfully synthesized the ternary alloyed $Zn_{1-x}Mn_xS$ nanowires with tunable composition ($0 \le x \le 1$) through the Ag_2S nanoparticle mediated growth. The composition, morphology and structure of the $Zn_{1-x}Mn_xS$ nanowires were determined by powder X-ray diffraction (XRD), high-resolution transmission electron microscopy (HRTEM), the inductively coupled plasma-mass spectrometry (ICP-MS), energy dispersive spectroscopy (EDS) and the electron paramagnetic resonance (EPR) analysis. The optical properties of the $Zn_{1-x}Mn_xS$ nanowires were investigated using the ultraviolet-visible (UV-Vis) and photoluminescence (PL) spectroscopies.

Experimental section

Materials

The used chemical reagents include $AgNO_3$ (99%), $Mn(NO_3)_2 \cdot 4H_2O$ (97.5%), $Zn(NO_3)_2 \cdot 6H_2O$ (98%), 1-dodecanethiol (98%), 1-dodecylamine (CP), dibutylamine (99%), methanol (99.7%), ethanol (99.7%), carbon disulfide (AR), NaOH (96%), HNO_3 (65–68%), cyclohexane (99.5%). These reagents were used as received without any further purification. And the deionized

[a]School of Materials Science and Engineering, Anhui Provincial Key Laboratory of Advanced Functional Materials and Devices, Hefei University of Technology, Hefei 230009, P. R. China. E-mail: caijs@hfut.edu.cn; ycwu@hfut.edu.cn

[b]Key Laboratory of Mesoscopic Chemistry of MOE, School of Chemistry and Chemical Engineering, Nanjing University, Nanjing 210093, P. R. China. E-mail: wangxzh@nju.edu.cn

† Electronic supplementary information (ESI) available: Additional (HR)TEM images, statistical distribution data, PL and EPR data of typical samples. See DOI: 10.1039/c7ra12714f

ultrapure water were collected from Milli-Q Advantage, Millipore.

Synthesis of the $[(C_4H_9)_2NCS_2]Ag$, $[(C_4H_9)_2NCS_2]_2Zn$ and $[(C_4H_9)_2NCS_2]_2Mn$ precursors and Ag_2S nanoparticles. The approaches of synthesis of metal dibutyldithiocarbamate complexes $[(C_4H_9)_2NCS_2]Ag$, $[(C_4H_9)_2NCS_2]_2Zn$, $[(C_4H_9)_2NCS_2]_2$-Mn precursors and Ag_2S nanoparticles have followed the similar procedures as reported in our previous study.[16,25]

Synthesis of the $Zn_{1-x}Mn_xS$ ($0 \leq x \leq 1$) nanowires. In a typical preparation, the metal dibutyldithiocarbamate complexes $[(C_4H_9)_2NCS_2]_2Zn$ and $[(C_4H_9)_2NCS_2]_2Mn$ precursors with the feeding molar fraction of Mn/(Mn + Zn) precursors, *i.e.* $[(C_4H_9)_2NCS_2]_2Mn/\{[(C_4H_9)_2NCS_2]_2Mn + [(C_4H_9)_2NCS_2]_2Zn\}$, at 0%, 12.5%, 25%, 37.5%, 50%, 62.5%, 75%, 87.5% and 100% were added into a round bottom flask, respectively. Then the mixed solvent of 1-dodecylamine and 1-dodecanethiol with the volume ratio of 1 : 1, and the Ag_2S nanoparticles suspension in cyclohexane with fixed amount, were all added into the flask. Then this mixture solution were stirred at 40 °C for 10 min by a magnetic stirrer. After that the flask were pumped, and quickly heated to 120 °C and kept there for 10 min. Following on, the products were carefully washed and centrifugalized with methanol and cyclohexane respectively for at least five times. Finally the solid products from the centrifuge were collected and dried for further characterization.

Characterization. The products were identified by X-ray diffraction (XRD, Cu target, $\lambda_{K\alpha} = 1.5418$ Å) with the step size of 0.02° and scan speed of 0.5 s per step. Their morphology, structure and composition were characterized by high resolution transmission electron microscopy (HRTEM, JEM-2100F) attached with an energy dispersive spectroscopy (EDS). Their composition were also determined using the inductively coupled plasma-mass spectrometry (ICP-MS, Agilent 7500), and before ICP-MS analysis, the samples were first dissolved by 10 mL 7% HNO_3 solution and then diluted to 80 mL using 2% HNO_3 solution. The absorption spectra were recorded by an ultraviolet-visible absorption spectrometer (UV-Vis, Rayleigh WFX-120B). The photoluminescence (PL) spectra were collected by laser confocal photoluminescence microscopy (LabRam HR Evolution) at room temperature with the 532 nm laser as the excitation source, and the products were scattered and flattened on a glass wafer before analysis. The electron paramagnetic resonance (EPR) experiments were performed on an X-band Bruker EMX spectrometer.

Results and discussions

The Ag_2S nanoparticles were prepared similarly to our previous reports,[16,25] the morphology and structure of the nanoparticles were characterized by (HR)TEM as shown in Fig. S1a–c.† The diameters of the Ag_2S nanoparticles were uniform with the average size of *ca.* 12.6 ± 1.7 nm as shown by Fig. S1d.† All of these obtained Ag_2S nanoparticles were stocked in cyclohexane for further use.

In the preparation of ternary $Zn_{1-x}Mn_xS$ nanowires, the $[(C_4H_9)_2NCS_2]_2Zn$ and $[(C_4H_9)_2NCS_2]_2Mn$ precursors with specific molar fraction of Mn/(Mn + Zn) at 0%, 12.5%, 25%, 37.5%, 50%, 62.5%, 75%, 87.5% and 100% were respectively mixed with unchanged amount of Ag_2S catalysts and the solvent of 1-dodecylamine and 1-dodecanethiol. Then after reaction, the nine products were collected and labelled as 1# to 9#, respectively. The XRD patterns of these samples have been shown in Fig. 1. It can be seen that the pattern of sample 1# coincided with the hexagonal ZnS phase (JCPDS: 36-1450), and that of sample 9# was consistent with the hexagonal γ-MnS phase (JCPDS: 40-1289). The diffraction peaks in 2–8# exhibited similar patterns to those of 1# (ZnS) and 9# (MnS). Meanwhile the corresponding single peak, such as the [110] peak, of the nine samples evolved progressively from the high 2θ angle towards the low 2θ angle from samples 1# to 9#, suggesting their increased lattice parameters (Table S1†). This result indicated that the samples 2–8# were composed of alloyed $Zn_{1-x}Mn_xS$ phase instead of phase-separated phases. And because the lattice constant of MnS is larger than that of ZnS, the increased lattice constants from 1–9# could be attributed to the increased Mn^{2+} concentration in the samples from 1–9#. Besides, the x values can be estimated following the eqn (1) based on the Vegard's law,[34]

$$x = \frac{a_x - a_{ZnS}}{a_{MnS} - a_{ZnS}} \quad (1)$$

where a_{MnS}, a_{ZnS} and a_x are the lattice parameters of hexagonal MnS, ZnS and $Zn_{1-x}Mn_xS$, respectively. The calculated x values were 0.10, 0.23, 0.32, 0.47, 0.64, 0.70 and 0.83 for samples 2–8#, respectively.

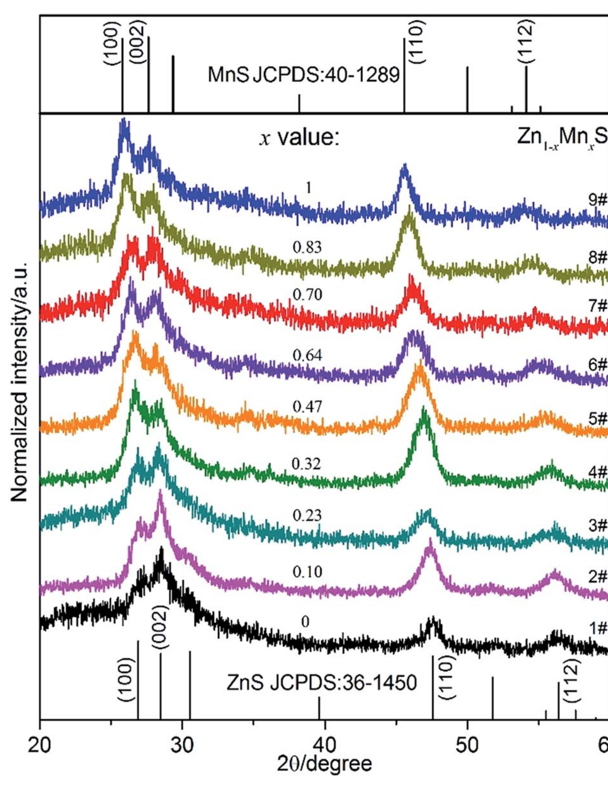

Fig. 1 XRD patterns of the samples 1–9#. The standard ZnS pattern (JCPDS: 36-1450) and MnS pattern (JCPDS: 40-1289) were shown on the bottom and top, respectively.

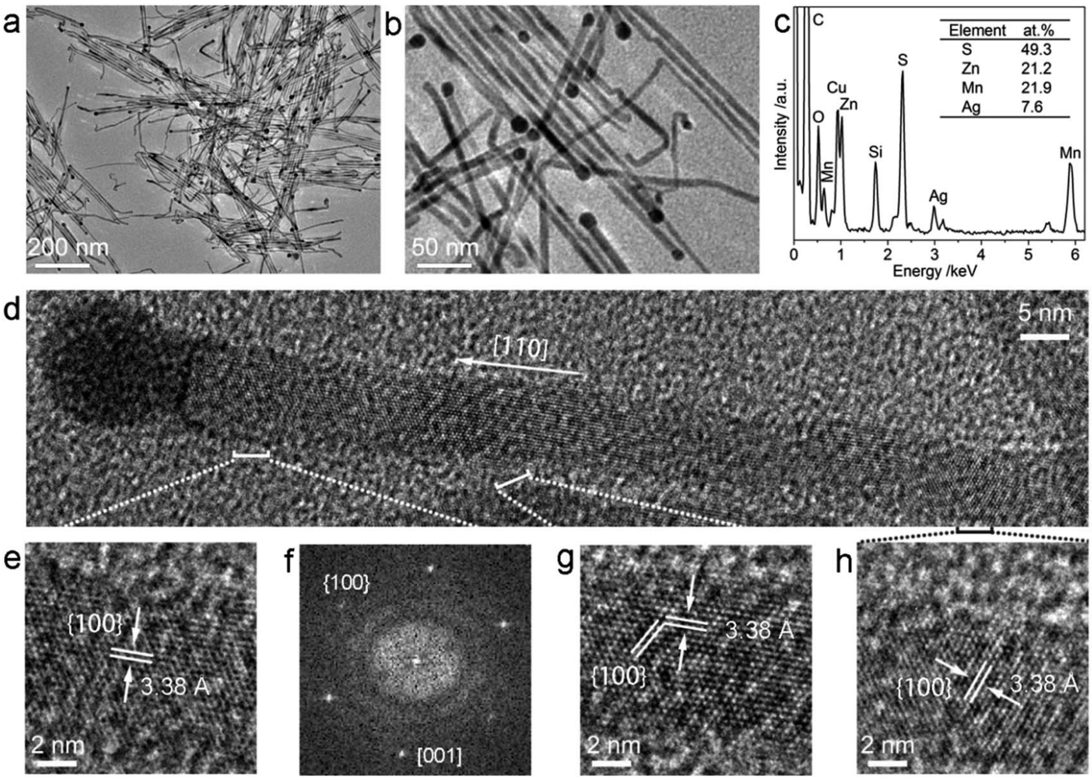

Fig. 2 (a, b) TEM images of the sample 5# with different magnification. (c) EDS spectrum of sample 5#. The C, O, Cu and Si signals come from the Cu grid. (d) HRTEM image of a typical heteronanostructure. (e, g, h) Enlarged HRTEM images from different sites of the $Zn_{1-x}Mn_xS$ nanowire in (d) as indicated by the dashed line. (f) Corresponding Fast Fourier Transform (FFT) pattern of the area in (e).

The morphologies of the samples 1, 3, 5, 7, 9# were characterized by the TEM microscopy as shown in Fig. S2,† 2a and b. It can be seen that the products were composed of matchstick-like heteronanostructures, which were constructed by a nanowire stem and a terminated nanoparticle. The average diameters of nanowires were *ca.* 6.5 ± 1.4 nm, 6.9 ± 1.0 nm, 6.9 ± 1.2 nm, 6.9 ± 1.3 nm, 6.7 ± 1.3 nm for samples 1, 3, 5, 7, 9#, respectively, without consideration of the terminated nanoparticles (Fig. S2†). The sample 5# was selected as the typical example for further analysis. EDS result (Fig. 2c) indicated that the Zn, Mn, Ag and S elements existed in the sample 5#, and the atomic ratio of elements Zn to Mn was 21.2 : 21.9 (inset of Fig. 2c), coincided well with $Zn_{0.53}Mn_{0.47}S$ phase as indicated by the XRD analysis (Fig. 1). Fig. 2e, g and h showed that the measured interplanar distances of the nanowire was 3.38 Å coinciding well with the d_{100} spacing (3.373 Å) of $Zn_{0.53}Mn_{0.47}S$ phase (Table S1†), and the growth direction of the nanowire was along [110] direction, which were also supported by the FFT pattern of the nanowire (Fig. 2f). However, this nanowire was not straight but seemed flexible, thus the direction of the lattice fringes with the same Miller index slightly changed along the nanowire as shown in Fig. 2g and h. Nevertheless, the interplanar distances along the nanowires (Fig. 2e, g and h) were unchanged which indicated the homogeneous composition along the nanowire, otherwise different interplanar distance could be found for the planes with the same Miller indices. Fig. S3† indicated that the terminated nanoparticle was composed of monoclinic Ag_2S phase (JCPDS: 14-0072). These results suggested the formation of ternary alloyed $Zn_{0.53}Mn_{0.47}S$ nanowire catalyzed by the Ag_2S nanoparticle for sample 5#. And it could also suggest that the Ag_2S nanoparticles can act as the catalysts for the growth of

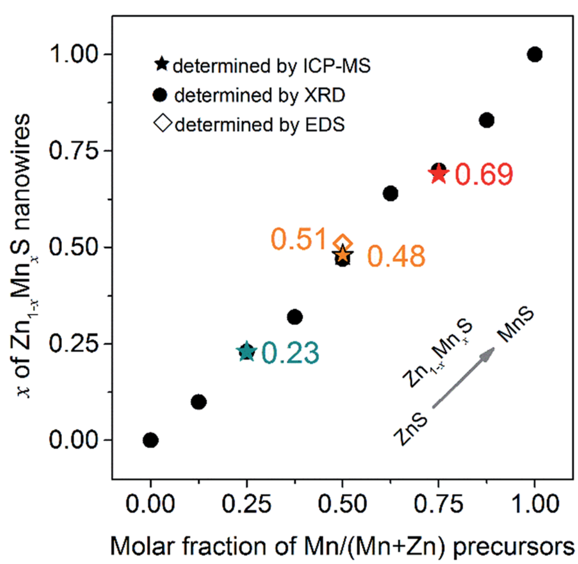

Fig. 3 The relationship between the experimental measured compositions x of $Zn_{1-x}Mn_xS$ nanowires and feeding molar fraction of Mn/(Mn + Zn) precursors. The compositions for samples 3, 5, 7# denoted by pentagon (★) were determined through ICP-MS, for all samples by dot (●) were determined through Vegard's law, and for sample 5# by diamond (◇) was determined through EDS analysis.

ternary $Zn_{1-x}Mn_xS$ nanowires *via* SSS route in this case, similar to the reported Ag_2S nanoparticles catalyzed growth of ZnS and MnS nanowires.[16,24,25,35]

To obtain the accurate composition x of $Zn_{1-x}Mn_xS$ nanowires, the typical samples 3, 5, 7# were characterized by ICP-MS and the molar fraction of Mn/(Mn + Zn) was measured at 0.23, 0.48 and 0.69, respectively (denoted by ★ in Fig. 3). Besides, the composition x for all samples determined by Vegard's law based on the XRD spectra were also drawn in Fig. 3 (denoted by ●), as well as the composition for sample 5# determined by EDS analysis (denoted by ◇). It can be seen that all these analysis methods have provided the similar results, indicating the x values determined by Vegard's law could be used to approximately represent their composition. In other words, the nanowires of samples 1–9# were composed of ZnS, $Zn_{0.90}Mn_{0.10}S$, $Zn_{0.77}Mn_{0.23}S$, $Zn_{0.68}Mn_{0.32}S$, $Zn_{0.53}Mn_{0.47}S$, $Zn_{0.36}Mn_{0.64}S$, $Zn_{0.30}Mn_{0.70}S$, $Zn_{0.17}Mn_{0.83}S$ and MnS phase, respectively. Besides, Fig. 3 has also shown that the experimental determined x values coincided well with the feeding molar ratio of Mn/(Mn + Zn) precursors, which suggested that this route was very effective in the synthesis of composition controlled $Zn_{1-x}Mn_xS$ nanowires.

The optical properties of these products were examined by UV-Vis and PL spectroscopies. The absorbance spectra of the samples in Fig. 4a all showed the discernible shoulder peaks. The bandgaps of the samples were extracted (Fig. 4b) using the method similar to the literatures.[20,36,37] It was interesting that the extracted bandgaps of $Zn_{1-x}Mn_xS$ nanowires did not shown a linear relationship with the composition x, but exhibited a nonlinear optical bowing effect (Fig. 4c) similar to that reported in PbS_xSe_{1-x} nanocrystals[38] and $ZnSe_xTe_{1-x}$ nanowires,[20] *etc.* Taking into accounts of the optical bowing effect, the quadratic eqn (2) below were used to fit the bandgaps of $Zn_{1-x}Mn_xS$ nanowires,

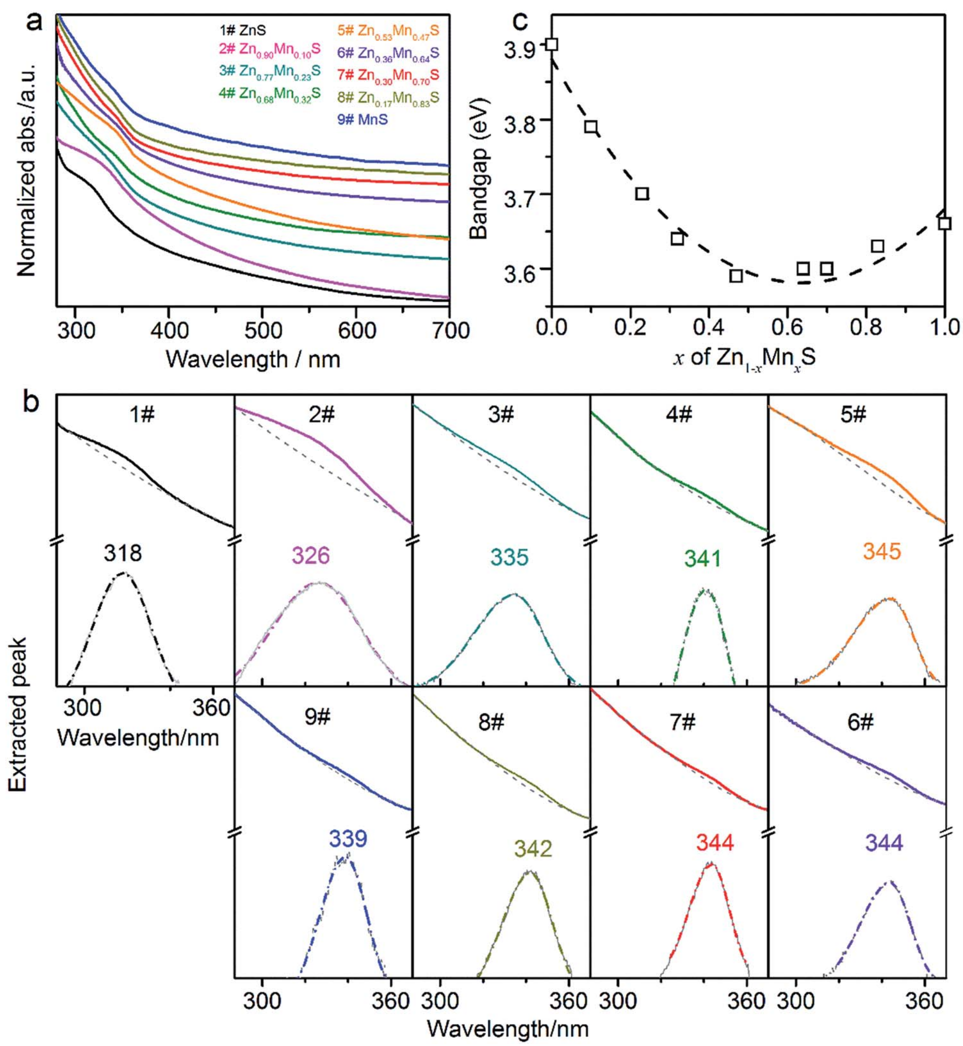

Fig. 4 (a) Absorption spectra of the typical samples 1–9#, which are denoted by different colors. (b) The extracted peaks for the samples 1–9#. For example, in the sample 1#, the top solid dark line was original absorbance curve. The top dashed grey line was the fitted baseline. The bottom solid grey peak was extracted by subtracting baseline from the absorbance curve. The bottom dashed dark curve was the fitted Gaussian plot, which displayed the shoulder peak located around 318 nm. The method to extract the shoulder peak was similar to that in the literatures.[20,36,37] (c) The relationship between the bandgap energy of $Zn_{1-x}Mn_xS$ nanowires and the composition x.

$$E_g\,(\text{eV}) = xE_g{}^{A} + (1-x)E_g{}^{B} - bx(1-x) \quad (2)$$

where $E_g{}^A$ and $E_g{}^B$ are the bandgaps of two binary phases A and B, b is the bowing parameter. Thus the bandgaps of the obtained $Zn_{1-x}Mn_xS$ nanowires was fitted as the eqn (3),

$$E_g\,(\text{eV}) = 3.88 - 0.94x + 0.74x^2 \quad (3)$$

where the fitted bowing character b was 0.74 ± 0.07 eV. The bowing effects, similar to the literatures,[20,38] could arise from the differences in electronegativities, atomic radii, and also the lattice constants between MnS and ZnS, and the larger differences may lead to the larger bowing parameters. Compared with the reported PbS_xSe_{1-x} nanocrystals[38] and $ZnSe_xTe_{1-x}$ nanowires[20] (Table S2†), the differences in electronegativities, atomic radii and lattice constants for the $Zn_{1-x}Mn_xS$ nanowires in this study are generally larger than those for PbS_xSe_{1-x} nanocrystals, but smaller than those for $ZnSe_xTe_{1-x}$ nanowires, which might render the $Zn_{1-x}Mn_xS$ nanowires exhibit a moderate b value among the three chalcogenide nanomaterials. The fitted equation gives the bandgap minimum of $Zn_{1-x}Mn_xS$ nanowires at $x = 0.64$, suggesting the bandgaps of $Zn_{1-x}Mn_xS$ nanowires ranging from 3.58–3.88 eV. This result indicated the SSS growth could be very effective in design the growth of $Zn_{1-x}Mn_xS$ nanowires with specific bandgap.

The PL properties of the samples 1, 3, 5, 7, 9# were examined (Fig. S4†) in the range of 550–850 nm using the 532 nm laser as the excitation source. It can be seen that the samples 1# (ZnS) and 9# (MnS) show featureless PL spectra, however, the ternary $Zn_{1-x}Mn_xS$ samples of 3, 5, 7# show clear characteristic yellow emission at 576 nm from the $^4T_1$–$^6A_1$ transition of Mn^{2+} dopant,[9] which indicated the formation of ternary alloyed $Zn_{1-x}Mn_xS$ compound. Besides, the EPR spectra of the typical samples of 3, 5, 7# were also collected as shown in Fig. S5.† The increased EPR intensity from samples 3# to 5# and 7# indicated the increased amount of Mn^{2+} in the $Zn_{1-x}Mn_xS$ nanowires, and the hyperfine structure of Mn^{2+} cannot be resolved due to the high Mn^{2+} concentration for these samples. These features are similar to those reported in $Cd_{1-x}Mn_xSe$ nanocrystals.[13] The results also supported the formation of ternary alloyed $Zn_{1-x}Mn_xS$ nanowires.

In conclusion, the ternary alloyed $Zn_{1-x}Mn_xS$ nanowires were controlled synthesized *via* the Ag_2S nanoparticle mediated growth under vacuum by the co-decomposition of $[(C_4H_9)_2NCS_2]_2Zn$ and $[(C_4H_9)_2NCS_2]_2Mn$ precursors. The diameters of the alloyed $Zn_{1-x}Mn_xS$ nanowires were uniform. The composition of the nanowires could be well tuned over the entire range ($0 \leq x \leq 1$). The relationship between the bandgaps and composition x of the $Zn_{1-x}Mn_xS$ nanowires were examined, and thus the bandgaps were found to exhibit the nonlinear bowing character *versus* the composition x. The results could provide new opportunities for modulating the bandgaps of Mn-based ternary chalcogenide nanowires and promote their further application in photonics and spintronics.

Conflicts of interest

There are no conflicts to declare.

Acknowledgements

This work was jointly supported by National Natural Science Foundation of China (No. 51602090, 51702077), Applied Technical Achievement Training Program of Hefei University of Technology (No. JZ2017YYPY0257), National Basic Research Program of China (No. 2013CB932902), and Foundation on the Integration of Industry, Education and Research of Hefei University of Technology (No. XC2015JZBZ18, XC2016JZBZ01).

Notes and references

1 N. Pradhan, S. Das Adhikari, A. Nag and D. D. Sarma, *Angew. Chem., Int. Ed.*, 2017, **56**, 7038–7054.
2 C. D. Pu, H. Y. Qin, Y. Gao, J. H. Zhou, P. Wang and X. G. Peng, *J. Am. Chem. Soc.*, 2017, **139**, 3302–3311.
3 Z. Deng, L. Tong, M. Flores, S. Lin, J. X. Cheng, H. Yan and Y. Liu, *J. Am. Chem. Soc.*, 2011, **133**, 5389–5396.
4 X. Yuan, S. H. Ji, M. C. De Siena, L. L. Fei, Z. Zhao, Y. J. Wang, H. Li, J. L. Zhao and D. R. Gamelin, *Chem. Mater.*, 2017, **29**, 8003–8011.
5 R. Beaulac, L. Schneider, P. I. Archer, G. Bacher and D. R. Gamelin, *Science*, 2009, **325**, 973–976.
6 X. Yuan, J. J. Zheng, R. S. Zeng, P. T. Jing, W. Y. Ji, J. L. Zhao, W. Y. Yang and H. B. Li, *Nanoscale*, 2014, **6**, 300–307.
7 H. Y. Chen, S. Maiti and D. H. Son, *ACS Nano*, 2012, **6**, 583–591.
8 E. Hofman, R. J. Robinson, Z. J. Li, B. Dzikovski and W. W. Zheng, *J. Am. Chem. Soc.*, 2017, **139**, 8878–8885.
9 S. L. Shen, Y. J. Zhang, Y. S. Liu, L. Peng, X. Y. Chen and Q. B. Wang, *Chem. Mater.*, 2012, **24**, 2407–2413.
10 M. A. Kamran, A. Majid, T. Alharbi, M. W. Iqbal, M. W. Amjad, G. Nabi, S. Zou and B. Zou, *J. Mater. Chem. C*, 2017, **5**, 8749–8757.
11 B. B. Srivastava, S. Jana, N. S. Karan, S. Paria, N. R. Jana, D. D. Sarma and N. Pradhan, *J. Phys. Chem. Lett.*, 2010, **1**, 1454–1458.
12 P. Arunkumar, K. H. Gil, S. Won, S. Unithrattil, Y. H. Kim, H. J. Kim and W. B. Im, *J. Phys. Chem. Lett.*, 2017, **8**, 4161–4166.
13 C. J. Barrows, P. Chakraboriy, L. M. Kornowske and D. R. Gamelin, *ACS Nano*, 2016, **10**, 910–918.
14 A. S. Silva, S. A. Lourenco and N. O. Dantas, *Phys. Chem. Chem. Phys.*, 2016, **18**, 6069–6076.
15 S. Joicy, R. Saravanan, D. Prabhu, N. Ponpandian and P. Thangadurai, *RSC Adv.*, 2014, **4**, 44592–44599.
16 Y. L. Zhang, J. Cai, T. P. Ji, Q. Wu, Y. Y. Xu, X. Z. Wang, T. Sun, L. J. Yang and Z. Hu, *Nano Res.*, 2015, **8**, 584–591.
17 Y. Liu, J. A. Zapien, Y. Y. Shan, C. Y. Geng, C. S. Lee and S. T. Lee, *Adv. Mater.*, 2005, **17**, 1372–1377.
18 Y. G. Chen, S. Zhao, X. Wang, Q. Peng, R. Lin, Y. Wang, R. A. Shen, X. Cao, L. B. Zhang, G. Zhou, J. Li, A. D. Xia and Y. D. Li, *J. Am. Chem. Soc.*, 2016, **138**, 4286–4289.
19 J. Pan, M. I. Utama, Q. Zhang, X. F. Liu, B. Peng, L. M. Wong, T. C. Sum, S. J. Wang and Q. H. Xiong, *Adv. Mater.*, 2012, **24**, 4151–4156.

20 F. J. Xu, B. Xue, F. D. Wang and A. G. Dong, *Chem. Mater.*, 2015, **27**, 1140–1146.
21 A. C. Onicha, N. Petchsang, T. H. Kosel and M. Kuno, *ACS Nano*, 2012, **6**, 2833–2843.
22 C. Y. He, Q. Wu, X. Z. Wang, Y. L. Zhang, L. J. Yang, N. Liu, Y. Zhao, Y. N. Lu and Z. Hu, *ACS Nano*, 2011, **5**, 1291–1296.
23 T. Kuykendall, P. Ulrich, S. Aloni and P. D. Yang, *Nat. Mater.*, 2007, **6**, 951–956.
24 L. Zhang, S. You, M. Zuo and Q. Yang, *Inorg. Chem.*, 2017, **56**, 7679–7686.
25 Y. L. Zhang, R. Xu, W. M. Chen, O. Zhuo, Q. Wu, J. Cai, X. Z. Wang and Z. Hu, *J. Mater. Chem. C*, 2017, **5**, 6493–6496.
26 G. X. Zhu and Z. Xu, *J. Am. Chem. Soc.*, 2011, **133**, 148–157.
27 S. L. Shen, Y. J. Zhang, L. Peng, Y. P. Du and Q. B. Wang, *Angew. Chem., Int. Ed.*, 2011, **50**, 7115–7118.
28 J. L. Wang, K. M. Chen, M. Gong, B. Xu and Q. Yang, *Nano Lett.*, 2013, **13**, 3996–4000.
29 W. W. Xu, J. Z. Niu, H. Z. Wang, H. B. Shen and L. S. Li, *ACS Appl. Mater. Interfaces*, 2013, **5**, 7537–7543.
30 J. C. Zhou, F. Huang, J. Xu and Y. S. Wang, *Nanoscale*, 2013, **5**, 9714–9719.
31 L. Zhang and Q. Yang, *Nano Lett.*, 2016, **16**, 4008–4013.
32 W. Han, L. X. Yi, N. Zhao, A. W. Tang, M. Y. Gao and Z. Y. Tang, *J. Am. Chem. Soc.*, 2008, **130**, 13152–13161.
33 J. L. Wang, C. M. Yang, Z. P. Huang, M. G. Humphrey, D. Jia, T. T. You, K. M. Chen, Q. Yang and C. Zhang, *J. Mater. Chem.*, 2012, **22**, 10009.
34 A. Denton and N. Ashcroft, *Phys. Rev. A*, 1991, **43**, 3161–3164.
35 F. D. Wang, A. G. Dong and W. E. Buhro, *Chem. Rev.*, 2016, **116**, 10888–10933.
36 F. D. Wang, R. A. Loomis and W. E. Buhro, *ACS Nano*, 2016, **10**, 9745–9754.
37 H. Yu, J. B. Li, R. A. Loomis, L. W. Wang and W. E. Buhro, *Nat. Mater.*, 2003, **2**, 517–520.
38 J. Akhtar, M. Afzaal, M. Banski, A. Podhorodecki, M. Syperek, J. Misiewicz, U. Bangert, S. J. O. Hardman, D. M. Graham, W. R. Flavell, D. J. Binks, S. Gardonio and P. O'Brien, *J. Am. Chem. Soc.*, 2011, **133**, 5602–5609.